Thin Solid Films 534 (2013) 673–679

Contents lists available at SciVerse ScienceDirect

Thin Solid Films

journal homepage: www.elsevier.com/locate/tsf

Modeling hydrogen permeation through a thin titanium oxide film and palladium

Z. Qin *, Y. Zeng [1], D.W. Shoesmith

The University of Western Ontario, London, Ontario, Canada N6A 5B7

ARTICLE INFO

Article history:
Received 28 June 2012
Received in revised form 6 February 2013
Accepted 8 February 2013
Available online 24 February 2013

Keywords:
Hydrogen permeation
Titanium oxide
Palladium
Thin film
Model simulation

ABSTRACT

Models that describe hydrogen permeation through a thin TiO_2 film deposited on Pd have been developed based on a mass-balance equation consisting of diffusion, reversible hydrogen absorption/desorption, and irreversible hydrogen trapping. These models were numerically simulated by the finite element method. By comparing model simulations with experimental permeation curves, values of the parameters associated with permeation, such as diffusion coefficients, absorption and desorption rate constants, trapping rate constants, and saturation concentrations, can be evaluated. The TiO_2 film noticeably impedes hydrogen permeation, essentially due to slow hydrogen transport in the oxide. The diffusion coefficient of hydrogen in TiO_2 was found to be 10^{-13} cm^2/s, three orders of magnitude lower than that in Ti metal.

1. Introduction

Titanium and its alloys have many industrial applications thanks to their excellent corrosion resistance and high specific strength. However, they are potentially susceptible to hydrogen-induced cracking (HIC) as a consequence of hydrogen absorption [1]. Hydrogen absorbed into Ti-alloys results in the formation of hydrides and fast crack growth which ultimately could lead to failure. Generally, titanium is covered by a passive titanium oxide (TiO_2) film. Though very thin (usually a few nanometers), this compact film acts not only as a protective layer against corrosion but also as a barrier to hydrogen absorption into the metal [2–5]. The impermeability of this film is, therefore, the limiting feature preventing HIC in Ti-alloys.

Hydrogen permeation through TiO_2 films is a complex process involving interfacial charge transfer, adsorption, absorption, trapping, and transport, and, thus, is inherently influenced by properties of the oxide, such as the chemical composition and structure, the presence of Ti^{n+} interstitials and/or oxygen vacancies, the type and concentration of impurities, hydrogen solubility, the adsorption characteristics of the surface, and the oxide thickness, porosity and uniformity [6]. The mechanism by which the oxide influences hydrogen permeation into Ti and its alloys is still not well established.

In aqueous solutions, measurable hydrogen absorption requires cathodic polarization leading to redox transformations within the oxide or the activation of "hydrogen windows" at defects in the film [7]. Torresi et al. [8] suggested that the activation energy for hydrogen evolution on passive titanium was much higher than on bare metal. Several studies [5,9,10] have shown that diffusion of hydrogen in TiO_2 is much slower than in Ti metal. Thus, the retardation of hydrogen permeation by TiO_2 films may be due to a combination of low hydrogen adsorption at the oxide surface and/or slow hydrogen transport in the oxide. In general, it is difficult to predict the rate of hydrogen transport through a TiO_2 film and how many hydrogen atoms, generated on the TiO_2 surface, reach the Ti substrate.

In this work, we present models for hydrogen permeation through a thin TiO_2 film deposited on Pd. These models are solved by the finite element method using COMSOL Multiphysics, and compared with experimental permeation measurements.

2. Experimental details

Due to complications caused by the formation of hydrides in Ti metal, a thin TiO_2 film deposited on a Pd foil was used, referred to as TiO_2/Pd. Pd was selected as the substrate because of its high solubility for hydrogen and rapid kinetics for hydrogen absorption and transport [11,12]. Thin TiO_2 films were deposited on Pd coupons of 0.1 mm thickness using thermal evaporation in a high vacuum system ($<2.0 \times 10^{-6}$ Pa). The deposition rate and thickness of the TiO_2 film were monitored and measured by a quartz crystal micro-balance.

A Devanathan [13] electrochemical cell was used to measure hydrogen permeation through TiO_2/Pd (Fig. 1). The TiO_2/Pd electrode is in the form of a membrane separating the cell into two compartments. Hydrogen is generated galvanostatically on the TiO_2/solution interface by water reduction, and a fraction of the hydrogen atoms produced is absorbed into the oxide. The hydrogen atoms then transport through the TiO_2/Pd membrane to be re-oxidized at the Pd/solution interface at a potential at which hydrogen oxidation is diffusion controlled.

* Corresponding author at: Department of Chemistry, Western University, London, Ontario, Canada N6A 5B7. Tel.: +1 519 6612111x86219; fax: +1 519 6613022.
E-mail address: zqin@uwo.ca (Z. Qin).
[1] Present address: Kinectrics Inc., Toronto, Ontario, Canada M8Z 6C4.

0040-6090/$ – see front matter © 2013 Elsevier B.V. All rights reserved.
http://dx.doi.org/10.1016/j.tsf.2013.02.030

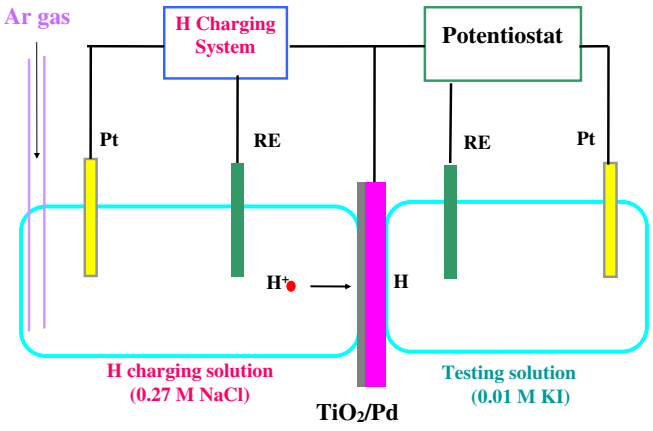

Fig. 1. TiO_2/Pd electrode acting as a membrane separating the Devanathan cell into two compartments: the left side of the membrane is galvanostatically charged, and the right compartment is potentiostatically maintained at 0.18 V_{SCE}.

The experimental procedures have been described in detail elsewhere [14].

The anodic current density (permeation current density) recorded at the Pd/solution interface represents the variation in the hydrogen flux exiting the TiO_2/Pd membrane, and thus provides a sensitive and convenient measure of the hydrogen permeation and diffusivity. Fig. 2 shows the permeation current densities at the charging current density of 80 nA/cm^2 through a Pd coupon and through Pd covered by a 24 nm thick TiO_2 film, while Fig. 3 shows the permeation current densities through the TiO_2-covered Pd at charging current densities of 80 nA/cm^2 and 40 nA/cm^2. These curves exhibit some typical features of a diffusion–absorption–trapping (DAT) process [15]. After the initiation of charging, the permeation current density remained at a steady, background value for a period (lag-time), t_L, before increasing, first rapidly, then more slowly to a steady-state value. Once steady-state was achieved, the charging current was switched off, and the permeation current density decreased back to the background value, but not immediately. It is clear from Fig. 2 that TiO_2 hinders hydrogen permeation significantly, the lag-time through the TiO_2-covered Pd being ~2.3 times longer than through Pd alone. The lag-time also depends on the charging current density (Fig. 3), being ~1.7 times longer at a charging current density of 40 nA/cm^2 compared to 80 nA/cm^2.

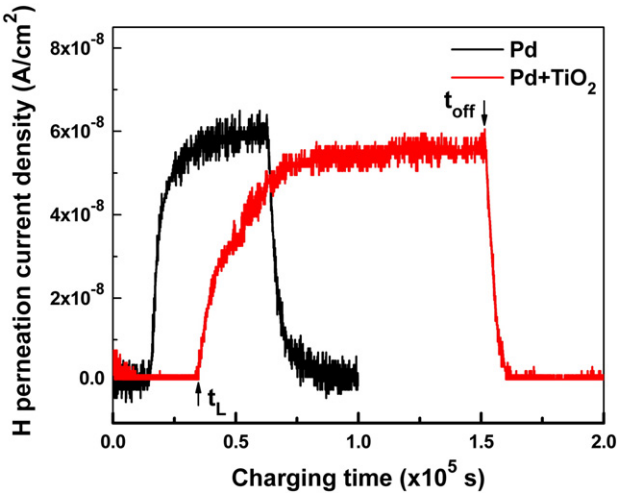

Fig. 2. Permeation current densities through Pd (–) and TiO_2-covered Pd (—) at a charging current density (i_0) of 80 nA/cm^2, where t_L is the lag-time and t_{off} is the time when the hydrogen charging current was switched off.

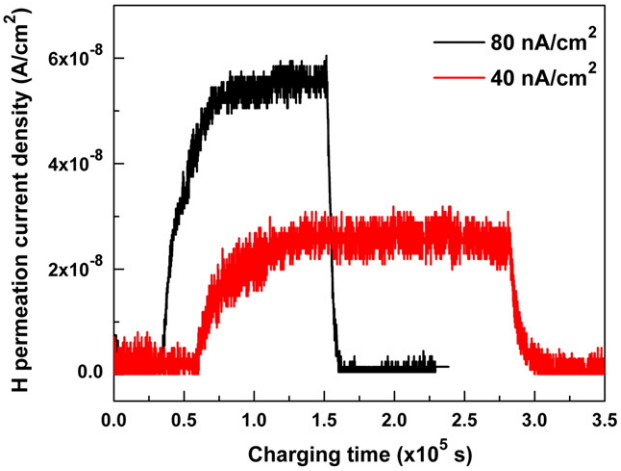

Fig. 3. Permeation current densities through TiO_2-covered Pd at charging current densities (i_0) of 80 nA/cm^2 (–) and 40 nA/cm^2 (—).

3. Permeation models

Early theoretical treatments for hydrogen permeation through a metal considered only diffusion [16–18]. Under such a simplification, the permeation current density, $i(t)$, is given by [19]

$$\frac{i(t)}{i_0} = f_H\left\{1-\frac{4}{\pi}\sum_{n=0}^{\infty}\frac{(-1)^n}{(2n+1)}\exp\left[-\frac{(2n+1)^2\pi^2 Dt}{4L^2}\right]\right\} \quad (1)$$

where i_0 is the charging current density, f_H is the charging efficiency defined as the ratio of the hydrogen produced to that absorbed, D is the hydrogen diffusion coefficient, F is the Faraday constant, and L is the thickness of the metal. The charging efficiency can be determined from the ratio of the steady-state permeation current density to the charging current density.

However, significant deviations were observed between experimental results and the diffusion-only model, because hydrogen may also be absorbed (reversibly trapped) and/or trapped (irreversibly) at defects or form hydrides [20–23]. McNabb and Foster [24] modified Fick's second law to include an absorption/desorption term, namely

$$\frac{\partial C}{\partial t}+N_r\frac{\partial n_r}{\partial t}=D\frac{\partial^2 C}{\partial x^2}$$
$$\frac{\partial n_r}{\partial t}=k_r C(1-n_r)-pn_r \quad (2)$$

where N_r is the number of absorption sites per unit volume, n_r is the fraction of these sites occupied, and k_r and p are the absorption and desorption rate constants, respectively. If absorption/desorption is much faster than diffusion, allowing the hydrogen to reach local equilibrium, they showed that, for low hydrogen concentrations, Eq. (2) could be reduced to the classical diffusion equation with D replaced by the apparent diffusivity, D_A, given by

$$D_A=\frac{D}{1+N_r k_r/p} \quad (3)$$

and hydrogen permeation in a system with absorption/desorption would behave similarly to that in an absorption-free system except that the hydrogen atoms appear to move a factor of $(1+N_r k_r/p)^{-1}$ slower.

The presence of defects, such as dislocations, grain boundaries, voids, and impurities, can act as traps for hydrogen in metal, since these sites have greater potential energy wells than those associated

with normal interstitial sites in the lattice [25,26]. The combined effects of absorption and trapping can be represented by Eq. (4) [27]

$$\begin{aligned}\frac{\partial C}{\partial t} &= D\frac{\partial^2 C}{\partial x^2} - N_r\frac{\partial n_r}{\partial t} - N_i\frac{\partial n_i}{\partial t}\\ \frac{\partial n_r}{\partial t} &= k_r C(1-n_r) - p n_r\\ \frac{\partial n_i}{\partial t} &= k_i C(1-n_i)\end{aligned} \tag{4}$$

in which N_i, n_i, and k_i are similar to the terms for absorption/desorption in Eq. (2), but refer to irreversible traps. When local equilibrium can be established and the fractional occupancies are very low, the apparent diffusion coefficient, D_{AT}, can be approximated by the equation

$$D_{AT} = D\left[\left(1+\frac{N_r k_r}{p}\right)\cdot\frac{3}{\kappa}\left(\frac{\sqrt{\kappa}}{\tanh\sqrt{\kappa}}-1\right)\right]^{-1} \tag{5}$$

where the trap strength, κ, is given by $N_i k_i L^2/D$. However, analytical solutions are not available for this generalized case incorporating both absorption and trapping [28].

The present model considers three processes, namely, (a) hydrogen diffusion, (b) reversible hydrogen absorption/desorption, and (c) irreversible hydrogen trapping as schematically illustrated in Fig. 4, and will consider permeation through both Pd and through TiO_2 covered Pd (TiO_2/Pd) in Sections 3.1 and 3.2, respectively.

3.1. Model for permeation through Pd

Before considering hydrogen permeation through an oxide film on Pd, it is necessary to first consider hydrogen permeation through Pd alone. Since the surface area of the Pd coupon is much greater than its thickness, a one-dimensional model is applicable. The mass balance equation accounting for the three processes can be written as

$$\frac{\partial}{\partial t}C_D(x,t) = D\frac{\partial^2}{\partial x^2}C_D(x,t) - \frac{\partial}{\partial t}[C_A(x,t)+C_T(x,t)] \tag{6}$$

where C_D, C_A, and C_T are the concentrations of diffusible (free), absorbed (reversible), and trapped (irreversible) hydrogen in Pd, respectively, and D is the hydrogen diffusion coefficient in Pd. The first term on the right-hand side of Eq. (6) represents the change in the concentration as a result of diffusion, while the second represents the change due to hydrogen absorption and trapping.

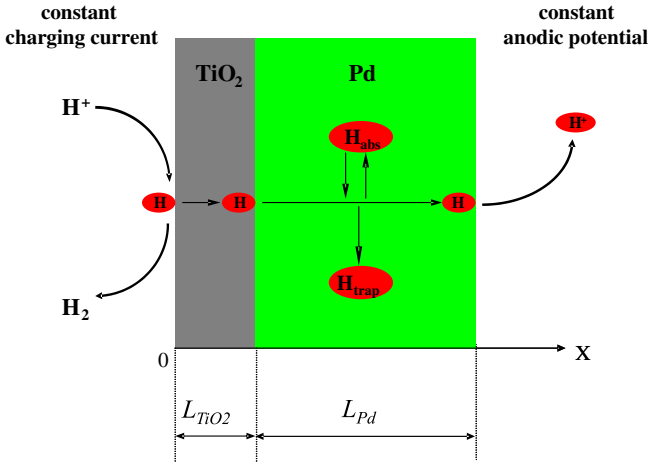

Fig. 4. Schematic illustration of hydrogen permeation through a TiO_2/Pd system.

Reversible absorption (hereafter referred to as absorption) is a dynamic process in which hydrogen absorbs and desorbs. The rate equation, assuming first order kinetics, can be written as

$$\frac{\partial}{\partial t}C_A(x,t) = k_A C_D(x,t) - k_D C_A(x,t) \tag{7}$$

where k_A and k_D are the rate constants for absorption and desorption, respectively. Trapping is an irreversible process, and its rate is assumed to be linearly proportional to the number of available trapping sites, *i.e.*

$$\frac{\partial}{\partial t}C_T(x,t) = k_T\left(1-\frac{C_T(x,t)}{C_T^S}\right)C_D(x,t) \tag{8}$$

where k_T is the trapping rate constant, and C_T^S is the saturation concentration of trapped hydrogen.

The two surfaces of the Pd coupon are either galvanostatically or potentiostatically controlled, yielding the boundary conditions,

$$\begin{aligned}-D\frac{\partial}{\partial x}C_D(x=0,t) &= f_H\frac{i_0}{F}\\ C_D(x=L,t) &= 0\end{aligned} \tag{9}$$

where L is the thickness of the Pd coupon. Initially, the coupon is free of hydrogen, *i.e.*

$$C_D(x,t=0) = C_A(x,t=0) = C_T(x,t=0) = 0. \tag{10}$$

Once steady state is established, the charging current is turned off, and the hydrogen absorbed during charging begins to be released. During this discharge period, the mass balance is governed by

$$\frac{\partial}{\partial t}C_D(x,t) = D\frac{\partial^2}{\partial x^2}C_D(x,t) - [k_A C_D(x,t) - k_D C_A(x,t)]. \tag{11}$$

Eq. (11) does not contain a trapping term because this process is irreversible, and does not occur after all available sites have been filled. During a discharge period, the hydrogen will be released from both sides of the Pd coupon under the conditions,

$$C_D(x=0,t>t_c) = C_D(x=L,t>t_c) = 0 \tag{12}$$

where t_c is the charging time.

3.2. Model for permeation through TiO_2-covered Pd

For simulations dependent on meshing, such as finite element methods, difficulties are often encountered in models containing thin layers since large geometric scale variations are present (in the present case a 24 nm film on a 0.1 mm thick Pd substrate). Three approaches have been attempted. The first approach used actual dimensions but different mesh densities in the TiO_2 and Pd. Simulations appeared to yield reasonable results for certain parameter values but not for others. The second approach used different length scales in the TiO_2 and Pd subdomains, with the diffusion and absorption parameters normalized accordingly. However, normalization of the flux is ambiguous at the TiO_2/Pd interface. To overcome this difficulty due to the large differences in dimensions of the TiO_2 film and Pd, the thin-layer approximation was applied, in which the thin TiO_2 film is replaced by a boundary layer sandwiched between a hypothetical fast diffusion layer (FDL) and the Pd, as demonstrated in Fig. 5.

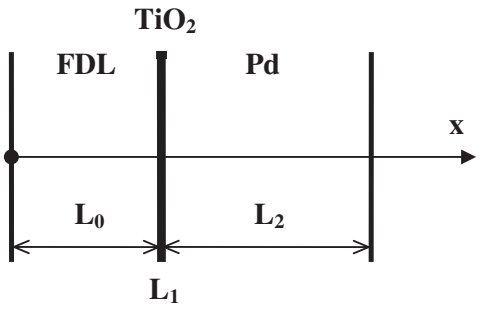

Fig. 5. Schematic illustrating the sandwich model in which the TiO_2 film is represented as a boundary layer between a fast diffusion layer (FDL) and the Pd substrate.

The FDL is a hypothetical layer in which diffusion is so fast that it has little effect on the subsequent TiO_2 and Pd, as given by

$$\frac{\partial}{\partial t}C_0(x,t) = D_0\frac{\partial^2}{\partial x^2}C_0(x,t) \quad (D_0 \gg D_1, D_2). \tag{13}$$

Hereafter, we use subscripts '0', '1' and '2' to refer to diffusional quantities in the FDL, TiO_2 and Pd, respectively.

Absorption and trapping are negligible in TiO_2 since it is very thin. Diffusion in TiO_2 is not explicitly treated, but incorporated as an interior boundary condition in the sandwich model. The flux at the interior boundary is approximated by the equation,

$$J_1(t) = -\frac{D_1}{L_1}\left(C_2\left(L_0^+,t\right) - C_0\left(L_0^-,t\right)\right) \tag{14}$$

where $C_0(L_0^-,t)$ and $C_2(L_0^+,t)$ are the concentrations at the left and right surfaces of the boundary layer, and D_1 and L_1 are the hydrogen diffusion coefficient and thickness of the TiO_2 layer, respectively. At the interior boundary the concentrations are discontinuous, and can be calculated using the built-in features of COMSOL Multiphysics. A similar approach has been applied in modeling contact resistances between metals [29]. The Pd is still governed by Eqs. (6)–(8), and the boundary conditions at the entrance and exit are as stated in Eq. (9).

After charging for a period of time, a steady state is achieved at which all concentrations are time-independent. At steady state, these concentrations can be determined analytically as

$$\begin{aligned} C_0^{ss}(x) &= \frac{f_H i_0}{F\cdot D_0}(L_0 - x) + \frac{f_H i_0}{F}\left(\frac{L_1}{D_1} + \frac{L_2}{D_2}\right) \\ C_2^{ss}(x) &= \frac{f_H i_0}{F\cdot D_2}(L_0 + L_2 - x) \\ C_A^{ss}(x) &= \frac{k_A}{k_D}C_2^{ss}(x); \quad C_T^{ss}(x) = C_T^S \end{aligned} \tag{15}$$

where C_0^{ss} is the steady state hydrogen concentration in the FDL, and C_2^{ss}, C_A^{ss}, and C_T^{ss} are the steady state concentrations of diffusible, absorbed, and trapped hydrogen in the Pd, respectively. Once steady state is established, the charging current is turned off. During the subsequent discharge period the TiO_2 film, though very thin, acts as a barrier that blocks hydrogen release from the TiO_2/Pd side. Therefore the boundary conditions during discharge are given by

$$\begin{aligned} &D_1\frac{\partial}{\partial x}C_1(x = L_0, t > t_c) = 0 \\ &C_2(x = L_0 + L_2, t > t_c) = 0. \end{aligned} \tag{16}$$

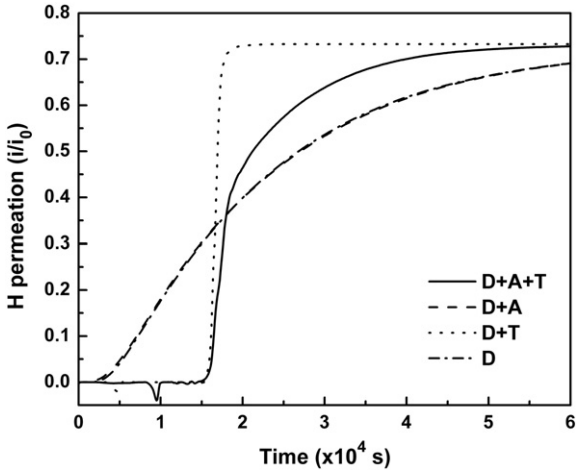

Fig. 6. Comparison of the simulation models: the present complete model (DAT), the diffusion and absorption model (DA), the diffusion and trapping model (DT), and the diffusion-only model (D).

3.3. COMSOL interface

Based on the mathematical models described above, a computer interface was built using the commercially available software, COMSOL Multiphysics (COMSOL Inc.). COMSOL Multiphysics is a modeling package based on the finite element method for the simulation of physical processes that are described by boundary-valued partial differential equations. The current simulations applied the Diffusion mode in the Chemical Engineering Module, COMSOL Multiphysics version 3.5.

4. Results and discussion

The present model includes three processes: diffusion, absorption and trapping. In Fig. 6, we compare the simulations of the present model (DAT) with the model (D) where only diffusion is included, the model (DA) where diffusion and absorption are included, and the model (DT) where diffusion and trapping are included. The simulation parameters are listed in Table 1. The parameter values are chosen one of two ways: (a) so that the simulated permeation (i) to charging current (i_0) ratios are equal at the half-height of the normalized steady-state current density for the DAT model (D and DA); (b) so that the model has the same lag time as the DAT model (DT). The simulations show that the D and DA models look very similar if the diffusion coefficient for the DA model is a factor $(1 + k_A/k_D)$ of that for the D model. They also show that trapping is primarily responsible for the lag-time. This comparison confirms that the modeling of hydrogen permeation requires all three processes, diffusion, absorption and trapping be taken into account.

Simulations using the complete model can now be compared with experimental permeation curves. The simulations were first applied to a Pd-only system to obtain the permeation parameters in Pd, and then extended to the TiO_2/Pd system to derive the parameters for the TiO_2 film. The values of simulation parameters are tabulated in Table 2. The values of D_0 and L_0 were selected so that the FDL had no effect on the simulation results of TiO_2/Pd.

Table 1
Simulation parameters for comparisons of the D, DA, DT, and DAT models.

Model	D_{Pd}	k_A	k_D	k_T	C_T^S
DAT	3.34×10^{-11} m^2/s	1 s^{-1}	0.0125 s^{-1}	10 s^{-1}	0.58 mol/m^3
DT	3.34×10^{-11} m^2/s	0	0	10 s^{-1}	0.957 mol/m^3
DA	3.34×10^{-11} m^2/s	1 s^{-1}	0.00625 s^{-1}	0	0
D	2.07×10^{-13} m^2/s	0	0	0	0

Table 2
Values of simulation parameters.

Symbol	Value	Description
i_0	8×10^{-4} A/m^2	Charging current density
f_H	0.6935	Charging efficiency
t_c	149000 s	Charging time
L_0	1×10^{-5} m	FDL thickness
L_1	2.4×10^{-8} m	TiO_2 thickness
L_2	0.0001 m	Pd thickness
D_0	1×10^{-5} m^2/s	Diffusion coefficient in FDL
D_1	1×10^{-17} m^2/s	Diffusion coefficient in TiO_2
D_2	3.34×10^{-11} m^2/s	Diffusion coefficient in Pd
k_A	1 s^{-1}	Absorption rate constant in Pd
k_D	0.0125 s^{-1}	Desorption rate constant in Pd
k_T	10 s^{-1}	Trapping rate constant in Pd
C_T^S	0.58 mol/m^3	Trapping saturation in Pd

The experimental and simulated permeation curves for Pd charging at 80 nA/cm^2 are compared in Fig. 7. The fit to the experimental curve is good, indicating that the model is a reasonable description of the permeation process. The charging efficiency f_H (0.7325) can be calculated from the ratio of the steady-state current density value and the charging current density. The diffusion coefficient obtained from the simulation, 3.34×10^{-7} cm^2/s, is consistent with published values [12,30]. No published data are available for comparison to the absorption/desorption rate constants, the trapping rate constant, and the trapping saturation in Pd. The ratio $k_A/k_D = 80$ indicates that the reversible absorption process is only slightly reversible, and may not be easily separable from the irreversible trapping process. The values of k_A and k_D were thus calculated from the discharge period where only reversible absorption is active. The values of k_T and C_T^S indicate that the Pd specimens have a number of traps that strongly interact with hydrogen. One possible source for such traps is the cold-working of the Pd foils during fabrication.

The experimental and simulated permeation curves for TiO_2/Pd charging at 80 nA/cm^2 are shown in Fig. 8. For the Pd part, the parameter values obtained from the Pd-only simulations were applied, on the assumption that the properties of the Pd are uninfluenced by the presence of the TiO_2 layer. The model simulation reproduced the experimental permeation curve reasonably well over the charging period, but a notable discrepancy was observed over the discharge period. During discharge, the TiO_2 film acts as a barrier to hydrogen release, allowing hydrogen release only from one side (*cf.* Eqs. (12) and (16)). Hence, discharge would be expected to be slower for TiO_2-covered Pd than for bare Pd. The observed steep decrease in i/i_0 without tailing cannot presently be explained, and requires further investigation.

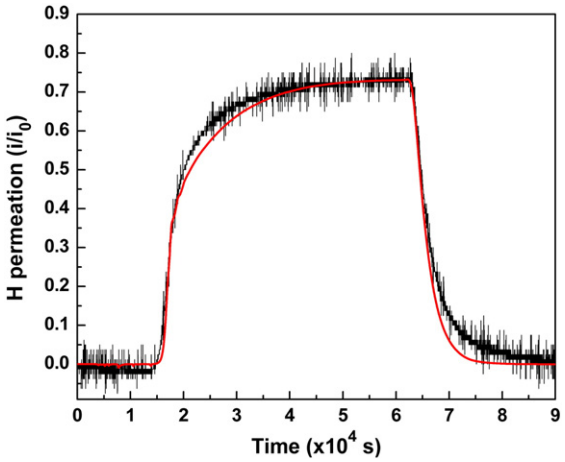

Fig. 7. A model simulation (—) compared to an experimental permeation curve (–) for Pd obtained at $i_0 = 80$ nA/cm^2.

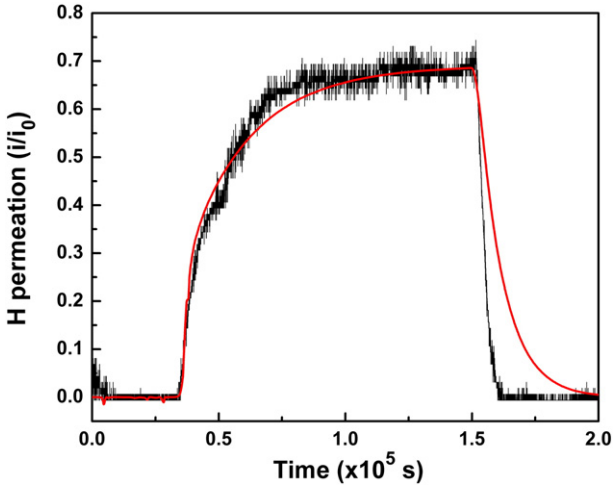

Fig. 8. A model simulation (—) compared to an experimental permeation curve (–) for TiO_2 deposited on Pd obtained at $i_0 = 80$ nA/cm^2.

Comparison to the Pd-only system shows that the TiO_2 film noticeably impedes hydrogen permeation. The charging efficiency for TiO_2/Pd (0.6935) is smaller than that for Pd (0.7325), indicating that a smaller fraction of the hydrogen produced on a TiO_2 surface is absorbed compared to that absorbed on a bare Pd surface. However, the most remarkable effect is in the time required for the permeation current density to start increasing and to achieve the steady state, which are both doubled for TiO_2/Pd compared to Pd. This suggests that hydrogen transport through the oxide rather than hydrogen evolution at the oxide surface is primarily responsible for the strong retardation of hydrogen permeation through TiO_2 films.

Since the permeation parameters are material specific, they should not be dependent on the charging current density. Therefore, the parameters determined by simulating the behavior at a charging current density of 80 nA/cm^2 should be able to simulate the behavior at a charging current density of 40 nA/cm^2. As shown in Fig. 9, the parameters obtained from the simulations at 80 nA/cm^2 fit well to the permeation curve charging at 40 nA/cm^2. Although the experimental permeation curves may appear quite different in 80 nA/cm^2 and 40 nA/cm^2 (Fig. 3), the permeation parameters remain unchanged as expected.

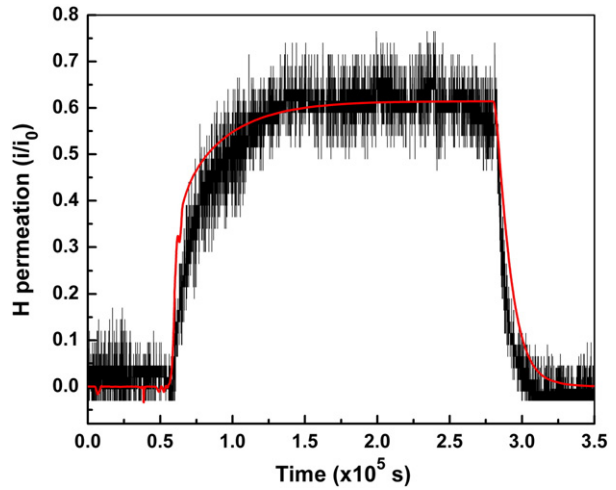

Fig. 9. A model simulation (—) compared to an experimental permeation curve (–) for TiO_2 deposited on Pd charging at $i_0 = 40$ nA/cm^2 using the parameter values determined from a simulation of the experimental curve obtained at 80 nA/cm^2.

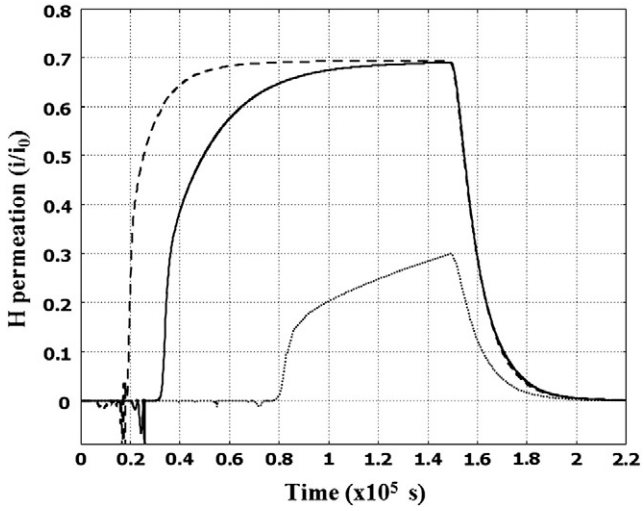

Fig. 10. Effect of diffusion in TiO_2 on permeation curves: (- -) $D_1 = 10^{-12}$ cm^2/s, (–) $D_1 = 10^{-13}$ cm^2/s, and (····) $D_1 = 10^{-14}$ cm^2/s (other simulation parameters are listed in Table 2).

The hydrogen diffusion coefficient in TiO_2 films, D_1, is one of the most important parameters in predicting HIC in Ti-alloys. The value of D_1 obtained in this study (10^{-13} cm^2/s) is three orders of magnitude lower than that in Ti metal [31]. This value is close to the value in TiO_2 films formed by plasma-enhanced chemical vapor deposition on Pd ($(3.9–5.2) \times 10^{-14}$ cm^2/s) [10], higher than that in thermally grown TiO_2 on pure titanium (2.84×10^{-16} cm^2/s) [4], and much higher than that obtained in single crystal rutile TiO_2 (7.5×10^{-20} cm^2/s) [5]. Our calculated value of D_1 can be regarded as an apparent or effective diffusion coefficient, which includes the influence of absorption and trapping in the oxide.

Fig. 10 shows the simulation results for various values of D_1, and demonstrates that hydrogen permeation is very sensitive to hydrogen diffusion in the oxide. The slower the diffusion through TiO_2, the longer the time-lag before permeation commences, and the longer the time required to achieve steady state. By comparison with the shape of the experimental permeation curve (Fig. 2), Fig. 10 also confirms that 10^{-13} cm^2/s is an optimized value in fitting the experimental data.

Model simulation can also provide information on H behavior in Pd that is otherwise experimentally difficult to obtain. For example, Fig. 11 exhibits time evolution of the profiles of diffusible, absorbed, and trapped hydrogen that were simulated by the model for TiO_2/Pd charging at 80 nA/cm^2. The identical shape of the profiles shown in Fig. 11a and b suggests that reversible absorption is fast, and, hence, always at local equilibrium. Fig. 11c shows that the front of trapped hydrogen moves with time as the trapping sites become filled up behind, until all sites have been filled. The fluctuations and values of C_T higher than the saturation capacity are due to non-physical numerical perturbations in the calculations. Fig. 11c shows that irreversible trapping sites are saturated after ~10 h, which is similar to the lag-time observed in the permeation current measurement (Fig. 2), indicating that trapping is primarily responsible for the lag-time.

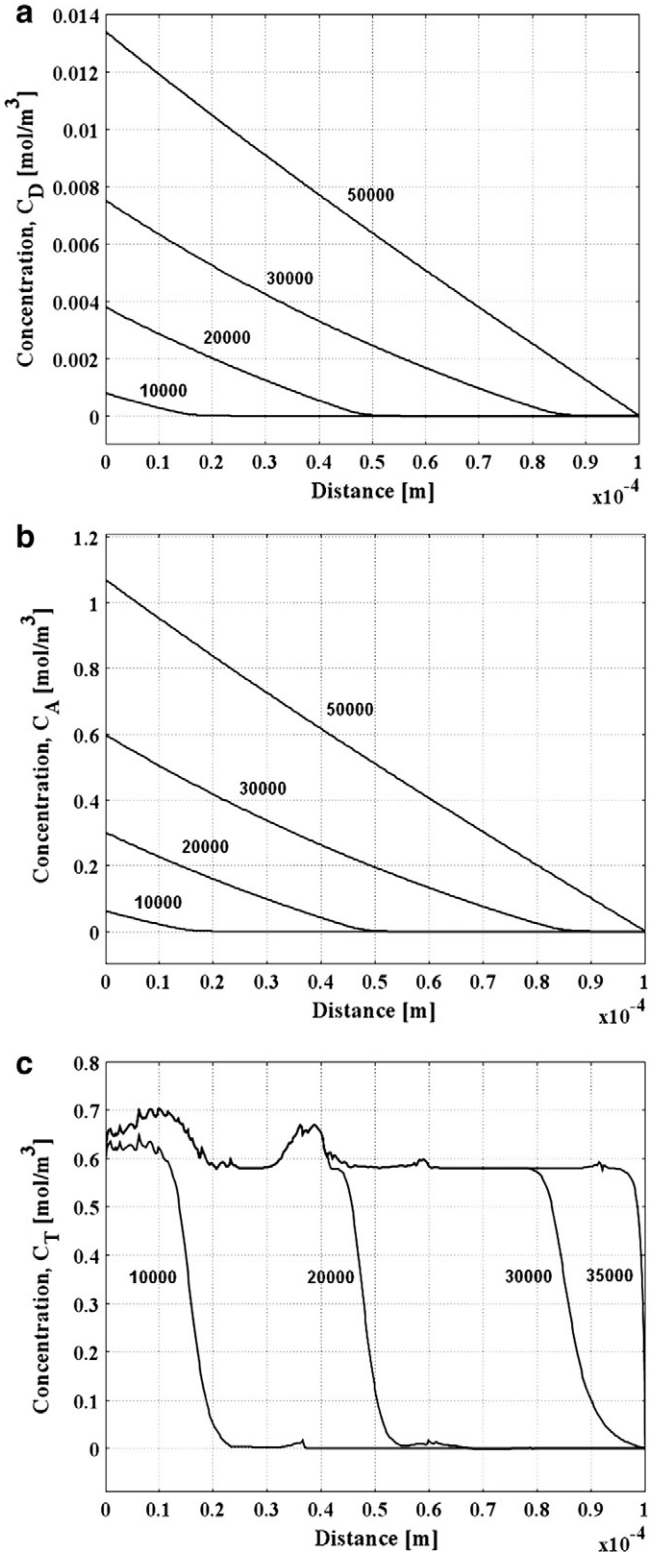

Fig. 11. Simulated hydrogen profiles as time evolves (as marked in seconds) for TiO_2/Pd charging at 80 nA/cm^2: (a) diffusible C_D, (b) absorbed C_A, and (c) trapped C_T.

5. Conclusions

Models describing hydrogen permeation through a thin TiO_2 film deposited on Pd were developed and solved using COMSOL Multiphysics. Comparison of simulated and experimental permeation curves shows that the models provide a better understanding of the mechanistic details of hydrogen permeation through oxide-covered Ti and yields values of the permeation parameters, such as diffusion coefficients, absorption and desorption rate constants, trapping rate constants, and saturation concentrations. While focused specifically on the TiO_2/Pd system, the models can be readily adapted to other thin film systems where permeation depends on diffusion, reversible absorption, and irreversible trapping.

Acknowledgments

This work was supported by the Natural Sciences & Engineering Research Council of Canada.

References

[1] Z. Qin, D.W. Shoesmith, J. Nucl. Mater. 379 (2008) 169.
[2] L. Yan, S. Ramamurthy, J.J. Noel, D.W. Shoesmith, Electrochim. Acta 52 (2006) 1169.
[3] Z. Tun, J.J. Noel, D.W. Shoesmith, J. Electrochem. Soc. 146 (1999) 988.
[4] S.K. Yen, Corros. Sci. 41 (1999) 2031.
[5] B.G. Pound, Corrosion 47 (1991) 99.
[6] B. Pound, Hydrogen Ingress During Corrosion, Corrosion and Oxide Films, WILEY-VCH, 2003, p. 118.
[7] F. Hua, K. Mon, P. Pasupathi, G. Gordon, D.W. Shoesmith, Corrosion 61 (2005) 987.
[8] R.M. Torresi, O.R. Camara, C.P. De Pauli, M.C. Giordano, Electrochim. Acta 32 (1987) 1291.
[9] G.R. Caskey, Mater. Sci. Eng. 14 (1974) 533.
[10] S. Pyun, J. Park, Y. Yoon, J. Alloys Compd. 231 (1995) 315.
[11] F.A. Lewis, J.P. Magennis, S.G. McKee, P.J.M. Ssebuwufu, Nature 306 (1983) 673.
[12] S.I. Pyun, Y.G. Yoon, Int. Mater. Rev. 45 (2000) 190.
[13] M.A.V. Devanathan, Z. Stachrski, Proc. R. Soc. 270 (1962) 90.
[14] Y. Zeng, J.J. Noel, P.R. Norton, D.W. Shoesmith, J. Electroanal. Chem. 649 (2010) 277.
[15] J.C. Wren, C.J. Moore, Z. Qin, Int. J. Mater. Eng. Technol. 3 (2010) 1.
[16] J. McBreen, L. Nanis, W. Beck, J. Electrochem. Soc. 113 (1966) 1218.
[17] N. Boes, H. Zuchner, J. Less-Common Met. 49 (1976) 223.
[18] J.G. Early, Acta Metall. 26 (1978) 1215.
[19] H.S. Carslaw, J.C. Jaeger, Conduction of Heat in Solids, Oxford Univ. Press, London, 1959.
[20] J. Won, S.I. Pyun, Electrochim. Acta 50 (2005) 1777.
[21] J.N. Han, M. Seo, S.I. Pyun, J. Electroanal. Chem. 499 (2001) 152.
[22] J.S. Chen, J.P. Diard, R. Durand, C. Montella, J. Electroanal. Chem. 406 (1996) 1.
[23] P. Millet, M. Srour, R. Faure, R. Durand, Electrochem. Commun. 3 (2002) 243.
[24] A. McNabb, P.K. Foster, Trans. Metall. Soc. AIME 227 (1963) 618.
[25] P. Buckley, J. Fagan, P. Searson, J. Electrochem. Soc. 147 (2000) 3456.
[26] S.B. Gesari, M.E. Pronsato, A. Juan, Int. J. Hydrog. Energy 34 (2009) 3511.
[27] M. Iino, Acta Metall. 30 (1982) 367.
[28] A. Turnbull, M.W. Carroll, D.H. Ferriss, Acta Metall. 37 (1989) 2039.
[29] COMSOL Support Knowledge Base No. 902, COMSOL Inc., 2008
[30] C. Gabrielli, P.P. Grand, A. Lasia, H. Perrot, J. Electrochem. Soc. 151 (2004) A1943.
[31] P.A. Sundaram, E. Wessel, H. Clemens, H. Kestler, P.J. Ennis, W.J. Quadakkers, L. Singheiser, Acta Mater. 48 (2000) 1005.